Microstructure and Mechanical Properties of Wear-Resistant Alloys Produced by the Laser Powder Bed Fusion Process

Kerri Horvay[1], Christopher Schade[1], Thomas Murphy[1], Corina Junghetu[2]

[1]Hoeganaes Corporation, Cinnaminson, NJ
[2]Hoeganaes Corporation Europe, Romania

ABSTRACT

Hard materials used in applications that require wear resistance typically are difficult to machine. Grinding is commonly used as a forming method, but it limits the part geometries that can be produced. By utilizing additive manufacturing as a forming method more complex geometries can now be achieved with a variety of hard tooling materials. For this study, the additive manufacturing technique laser powder bed fusion was used to process a series of wear-resistant alloys developed to provide a range of properties for different tooling applications. Microstructural and mechanical properties were evaluated for heat treated samples. Standardized wear testing was performed to correlate the wear resistance to the hardness of the material. The toughness of the materials was also evaluated for applications that require both wear resistance and impact resistance.

INTRODUCTION

Applications involving exposure to wear conditions such as fasteners, bearings, punches and dies require a material with good wear resistance. The wear of a material occurs when a solid surface is damaged by relative motion with a contacting surface [1, 2]. Scars of different shapes and sizes will form due the progressive loss of material from this damage. These material losses can eventually consume the part or deteriorate its function decreasing its performance. Abrasive wear, a common wear mechanism found in industrial applications, occurs when hard particles are forced against and move along a solid surface. The tendency for a surface to abrade depends on the characteristics of the surfaces, the presence of abrasives, speed of contact, and other environmental conditions [2]. Metals that will resist this abrasive wear generally have high hardness. Thus, heat treated carbon or alloy steels are generally used for wear and abrasion-resistant applications. Tool steels will have additional abrasion resistance from carbide formation. Material selection is important because no tool steel has maximum wear resistance, toughness, and heat softening resistance [1]. Generally, they must be heat treated to develop a targeted combination of wear resistance and toughness because there will be a tradeoff in properties. For applications such as pumps, valves and bearings the corrosion resistance of the alloy must also be considered [2].

In general hard materials for tooling and wear-resistant applications are very difficult to machine, with the most common forming method being grinding. However, this method has limited design freedom for components. By combining additive manufacturing with wear-resistant materials more complex geometries can now be produced. In a previous paper, a new family of alloys called AncorWear (AW) was introduced [3]. These materials were designed for the additive manufacturing (AM) process, laser powder bed fusion (LPBF), and cover a range of hardnesses comparable to wrought alloys that are available for wear-resistant applications. The microstructural and mechanical properties of the LPBF samples were presented in the previous paper as well as the results of a case study to determine how the AM production method would influence the performance of a part in service. Parts for a grinding mill with high wear exposure conditions were chosen to manufacture by LPBF with an AncorWear alloy as shown in Figure 1. The wear and damage to the LPBF parts were monitored as a function of the amount of material processed through the mill. The results were promising when comparing to the conventionally processed parts. To eliminate the need for such costly trials further investigation into the wear behavior of these alloys is needed. Thus, this study will investigate additional heat treatments to produce a wider range of mechanical properties, microstructural analysis and standardized wear testing of the AncorWear alloys.

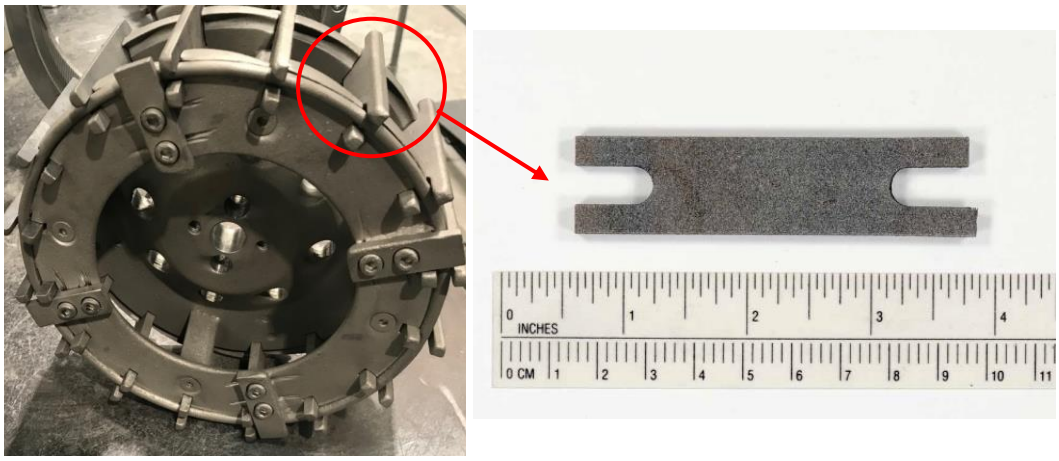

Figure 1. Grinding mill (left) and LPBF part (right) from case study in previous paper.[4]

EXPERIMENTAL PROCEDURE

The powders used in this study were screened to a nominal 15-53 µm particle size for LPBF processing. The chemical composition of the powders are listed below in Table I. AncorWear SS is a water atomized stainless steel that can be used in applications also requiring moderate corrosion resistance with abrasion resistance. The remaining steels were gas atomized with different carbon concentrations and alloying elements to provide a range of properties needed for different applications. AncorWear 500 and 600 are comparable to conventional wrought abrasion-resistant grades commonly produced in plate steels [3]. AncorWear SPL is a chromium/nickel free alloy designed to meet health and safety requirements where chromium and nickel are not permitted. AncorWear S7 is a tool steel that has good impact and shock resistance as well as good heat softening resistance.

Table I. Chemical composition of powders used in this study (wt.%).

Alloy	C	Cr	Ni	Mo	Mn	Si	V	Oxygen
AncorWear SS	0.02	11.85	1.05	0.22	0.14	0.88	---	0.25
AncorWear 500	0.17	0.66	0.70	0.61	1.39	0.50	---	0.02
AncorWear SPL	0.23	0.08	0.09	1.48	1.01	1.23	0.14	0.03
AncorWear 600	0.44	1.31	4.14	0.37	0.60	0.21	---	0.03
AncorWear S7	0.51	3.15	---	1.57	0.78	0.69	0.30	0.03

* *Each alloy has a balance of iron*

LPBF Processing

An EOS M290 machine was used to make the testing specimens by melting powder layer by layer with a Yb fiber laser (400 W) within an argon filled chamber. Samples (10 mm by 10 mm by 10 mm) were built with a variety of different settings to evaluate the porosity content produced with each alloy. A constant layer thickness was used for all the samples while the laser power, hatch distance, and scanning speed were varied. Image analysis, following MPIF standard guide 69, was used to measure the porosity content of the cross-sections of the cubes perpendicular to the build direction.[6] Light-optical microscopy (LOM) images of prepared cross-sections in the as-polished condition were taken. Settings were chosen for each alloy that led to a density greater than 99.0%.

Mechanical Testing

Mechanical testing specimens (conventional flat "dogbone" specimens per MPIF Standard 10 and v-notch charpy impact specimens per ASTM E23) were printed of each alloy [4,5]. Samples were printed vertically and cut from the build plate in the as-built condition. Then the specimens were heated to various temperatures for 1 hour followed by different cooling rates using a batch furnace with a nitrogen atmosphere. AW-SS had a two-step heat treatment to form a dual phase microstructure of martensite and ferrite. It was first heated to 1260 °C for 30 minutes in a hydrogen atmosphere and furnace cooled to room temperature. Then heated to 593 °C for 1 hour and furnace cooled to temper the martensite that was formed during the first step in the heat treatment. A light optical microscope and scanning electron microscope (SEM) were used to evaluate the microstructure of the samples.

Wear Resistance Testing

Wear testing to investigate the effect of scratching abrasion on each alloy was completed according to ASTM G65 Procedure A, "Standard Test Method for Measuring Abrasion Using the Dry Sand/Rubber Wheel Apparatus". This type of wear depends upon factors including the abrasive particle size, shape, hardness, frequency of contact, etc. [6]. This test can provide a relative ranking of materials tested, but cannot predict the exact wear resistance in a specific environment. A diagram of the test is shown in Figure 2a. A test specimen is pressed against a rotating wheel while an abrasive sand is flowed between the specimen and the wheel. Abrasion test samples (76 mm x 25 mm x 13 mm) of each alloy were printed vertically. They were cut from the build plate in the as-built condition and then heat treated before testing. Sand was flowed between the neoprene rubber wheel and specimen at a rate of 300-400 g/min with a test load of 133 N. The samples were subjected to 6000 cycles for a 30 minute duration. The mass of each sample was recorded before and after the test and then converted to volume loss. The hardness of the abrasion samples was also measured.

Wear testing to investigate the effect of sliding wear on each alloy was completed according to ASTM G99, “Standard Test Method for Wear Testing with a Pin-on-Disk Apparatus”. This type of wear depends on factors including the applied load, machine characteristics, sliding speed, sliding distance, the environment, and the material properties [7]. A diagram of the test is shown in Figure 2b. A ball (AISI 52100) with a 12.7 mm diameter was rigidly held and positioned perpendicular to a flat circular disk (diameter 54 mm by 9.5 mm). The ball was pressed against the disk at a load of 67 N and moved in a circular sliding path at 20 rpm. The test was completed at room temperature for a 60 minute duration. The amount of wear is determined by measuring the length or shape change of the ball and disk wear tracks. Disk samples were printed horizontally and cut in the as-built condition. The disk surfaces were machined to the specified thickness and then heat treated before testing. The diameter of the wear scar formed on the bar and the width of the wear scar formed on the disk were measured. The hardness of the disks was also measured. A SEM was used to observe the surface morphology of the wear tracks.

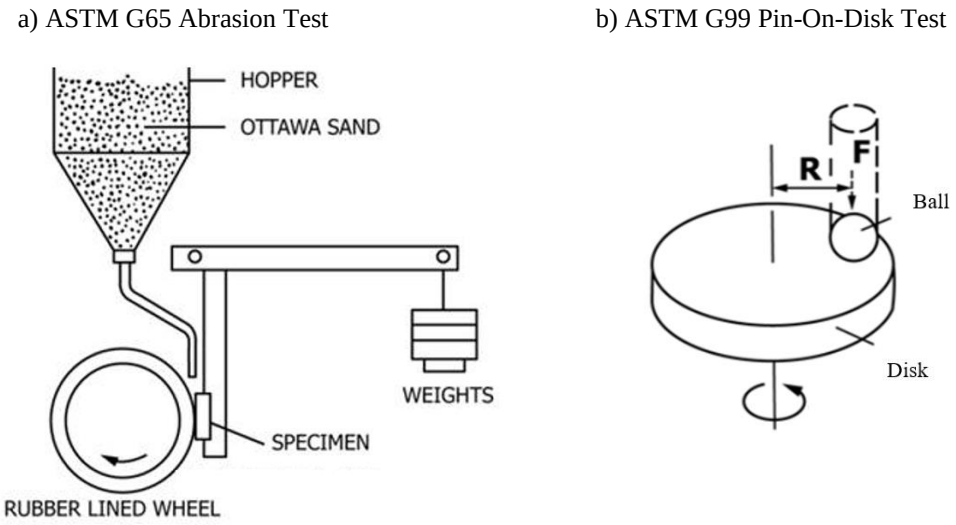

Figure 2. Diagrams of wear testing [6, 7].

RESULTS & DISCUSSION

LPBF Processing

Samples were printed of each alloy with a variety of settings. High density was achieved with a standard set of settings for each material. Microcracks were observed in the AW-S7 samples as shown in Figure 3. This was likely due to the high carbon and alloying content in this material resulting in crack formation during printing. Using a higher build plate temperature to decrease the steep thermal gradient could possibly reduce or eliminate the cracking in the printed AW-S7 material. There were no cracks observed in the other alloys. For comparison, an AW-600 sample cross-section is also shown in Fıgure 3.

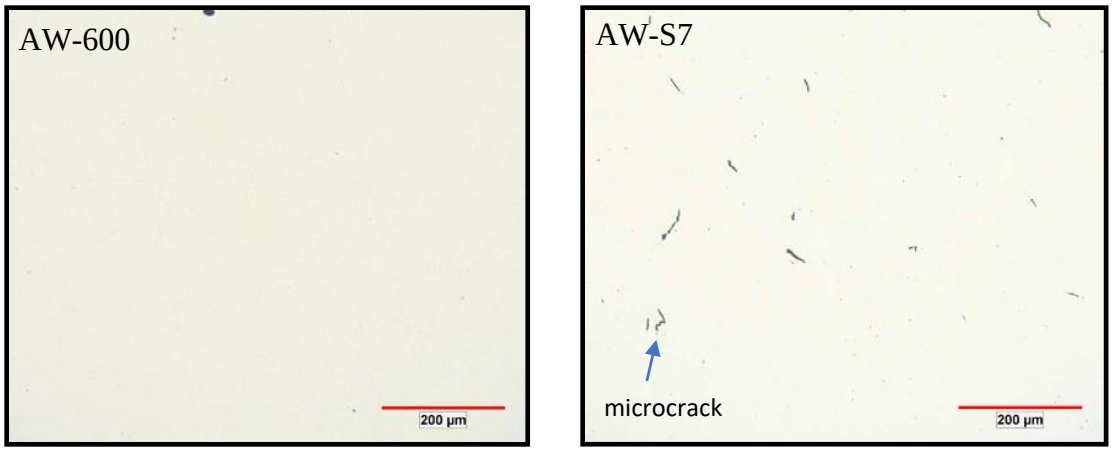

Figure 3. LOM images of AncorWear sample cross-sections in the as-polished condition.

Mechanical Testing

Different heat treatments were used to investigate the range of mechanical properties possible with each alloy. Three cycles were chosen as shown in Table II. For cycle 1 samples were tempered at 593 °C for 1 hour and then air cooled (AC). For cycle 2 samples were tempered at a higher temperature, 760 °C, to increase ductility and impact resistance. For cycle 3 samples were austenitized for 1 hour and oil quenched (OQ) to increase hardness [8]. Samples were then tempered at 204 °C in cycle 3 to stress relieve the transformation products formed after oil quenching.

Table II. Heat treatments cycles for LPBF samples.

Cycle	Temperature & Cooling Method
1	593 °C, air cool
2	760 °C, air cool
3	954 °C, oil quench; temper 204 °C, furnace cool

Tensile properties were measured on the heat treated AncorWear samples and summarized in Figure 4. A wide range of yield and ultimate tensile strength, elongation, and hardness were reached between the different alloys and heat treatments. The yield strength ranged from 393-1675 MPa while the ultimate tensile strength ranged from 572-1868 MPa. The highest elongation reached was 25.3% and the highest hardness reached was 53 HRC. Hardness and strength generally increased from materials with low carbon content to high carbon content while the elongation showed the opposite trend. The heat treatment cycles showed varying effects on the properties. Tempering with cycle 1 (593 °C, air cool) generally produced higher strength and hardness levels than tempering with cycle 2 (760 °C, air cool). Cycle 2 produced high elongation levels in all the alloys except for AW-600. AW-SS and AW-S7 showed a large increase in elongation with cycle 2 compared to the other cycles. Austenitizing and oil quenching with cycle 3 produced the highest strength levels and the lowest elongation levels. These results show that with each alloy a variation in properties is achieveable and by using an optimal heat treatment the properties can be further tailored.

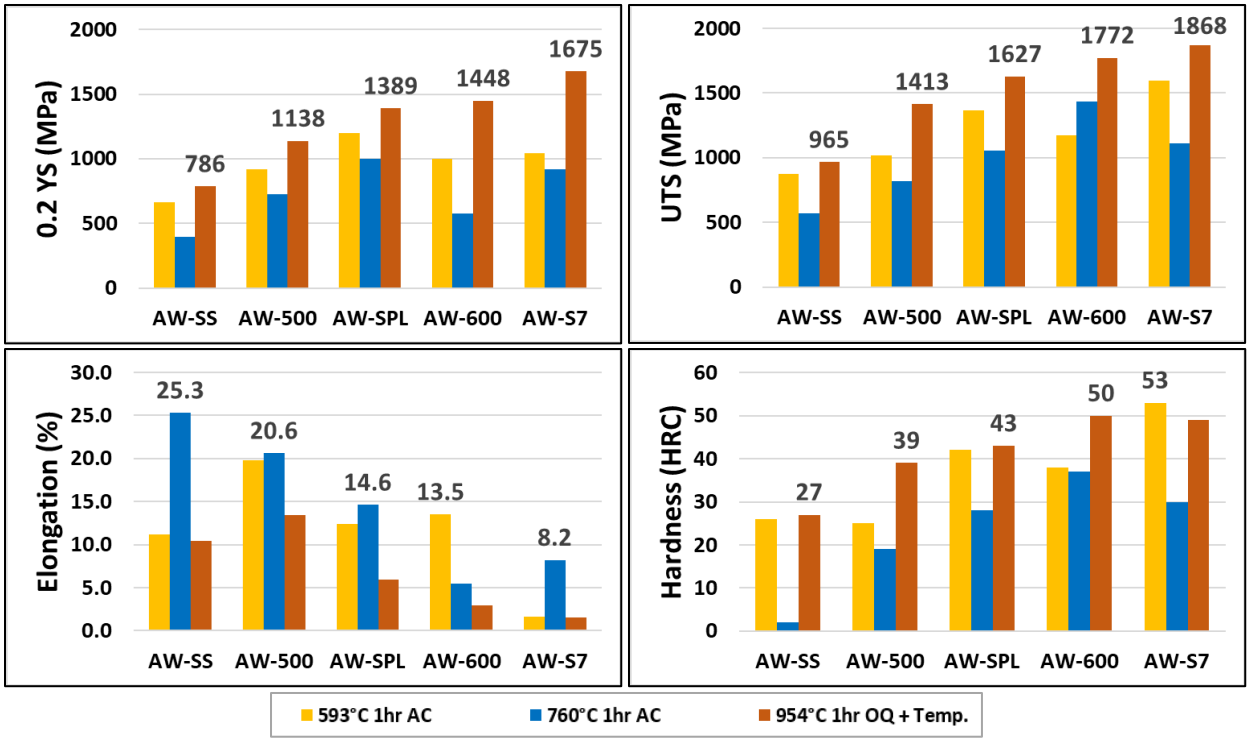

Figure 4. Summary of AncorWear tensile properties achieved by different heat treatments.

When plotting the ductility and strength levels of all the materials, as shown in Figure 5, the range of properties achieved can be observed. AW-SS achieved the highest elongation while AW-S7 reached the highest strength level. Depending on the part application increased hardness, toughness, ductility or corrosion resistance may be needed. This family of AncorWear alloys provides different materials for a wide range of properties for various applications.

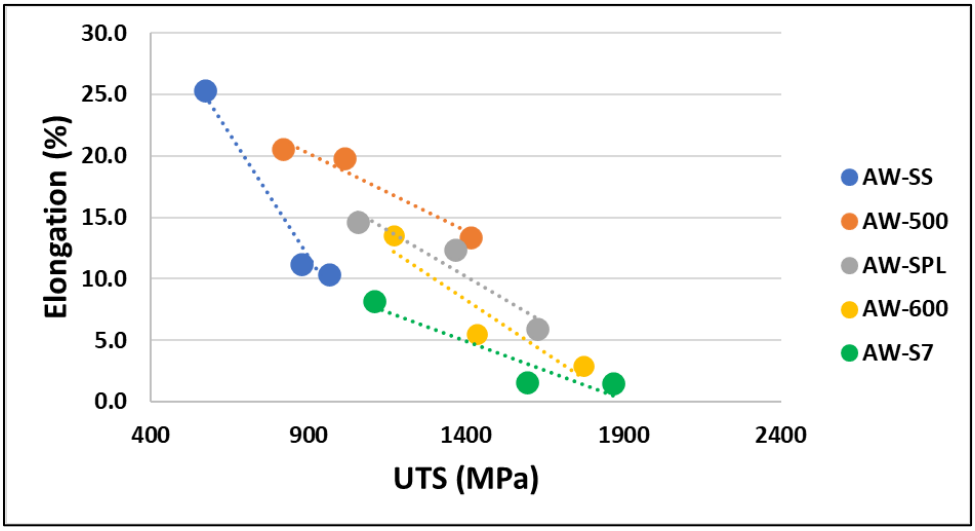

Figure 5. Ultimate tensile strength versus elongation of the heat treated AncorWear alloys.

Charpy Impact Testing

Charpy v-notch impact testing samples were also heat treated utilizing the same conditions as the tensile samples to investigate the toughness of the different alloys. Figure 6 shows the results from the charpy impact testing. AW-500 had the highest impact energy as compared to the other alloys. The highest impact energy for AW-500 was reached with cycle 2 (760 °C, air cool). The impact energy of the alloys generally decreased as hardness increased except for AW-SS. The austenitized and oil quenched samples showed the lowest impact energy condition for each alloy except for AW-SS. The AW-S7 charpy samples ranged from 4-12 J depending on the heat treatment. Comparatively, AISI S7 tool steel air cooled from 941 °C and tempered at 200 °C has a reported v-notch charpy impact value of 16.9 J [9]. The lower values compared to wrought may be due to the microcracks present in the AW-S7 samples from printing. Further investigation into the effect of printing the v-notch versus machining is needed to see how this could have impacted the results.

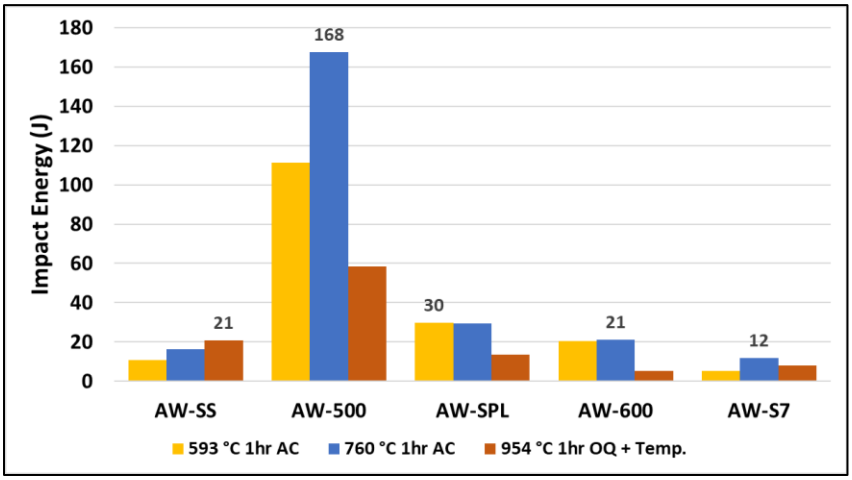

Figure 6. Summary of the heat treated AncorWear alloy impact energy results.

Figures 7 and 8 show the fracture surfaces of the charpy impact bars heat treated according to cycle 1. AW-SS and AW-S7 have the most flat surfaces indicative of brittle fracture [8]. This corresponds to their impact energies which were the lowest of the alloys with cycle 1. AW-600 and AW-SPL had the next highest impact energies and their fracture surfaces show signs of plastic deformation. AW-500 had the highest impact energy of the group and its surface showed the most plastic deformation. Additionally, an SEM image of the AW-500 sample shows a dimpled surface indicative of ductile fracture.

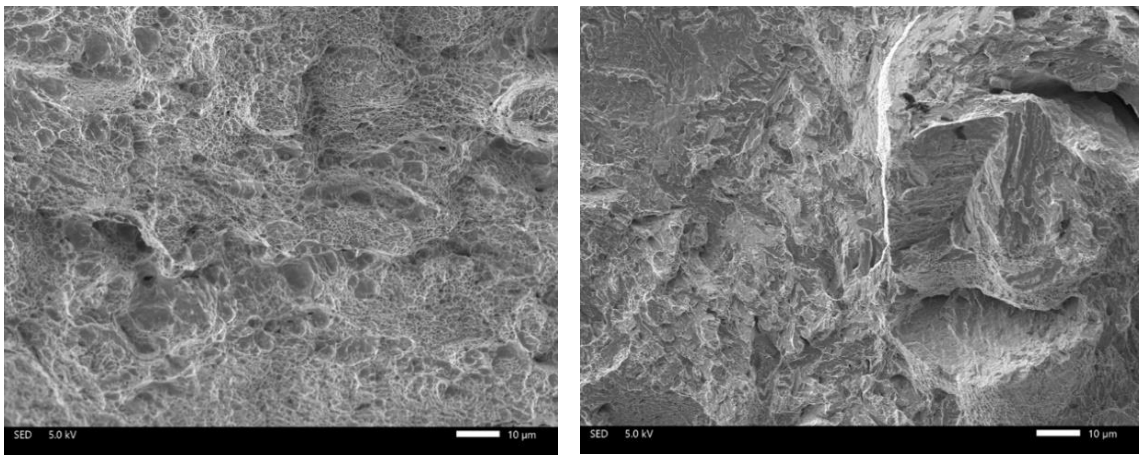

Figure 7. SEM images of AW-500 (left) and AW-S7 (right) fracture surfaces.

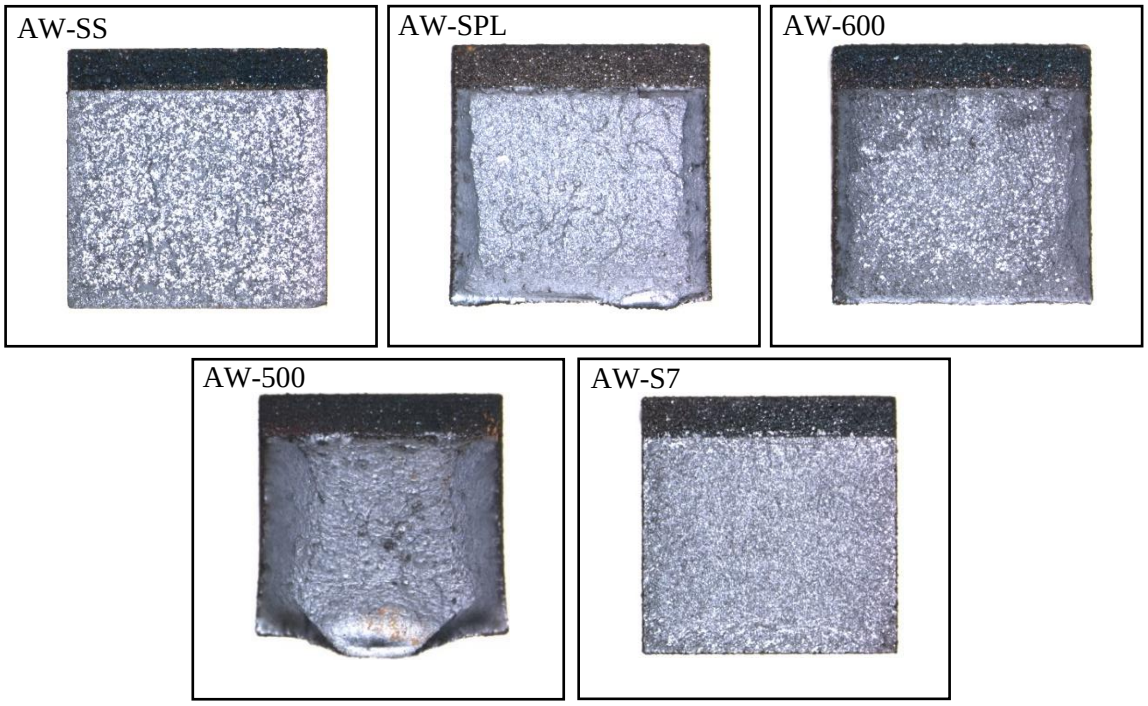

Figure 8. Impact bar fracture surfaces with cycle 1 heat treatment (593°C, air cool).

Metallography

Etched microstructures of the heat treated tensile samples with cycles 1, 2, and 3 are shown in Figure 9. AW-SS heat treated with cycle 1 is shown with a dual phase microstructure, which was achieved by heat treating in the two phase region (austenite/ferrite) followed by rapid cooling then tempering at 593°C [10]. The white areas are an interconnected ferrite matrix with islands of transformed austenite. AW-SS heat treated with cycle 2 has a ferritic structure with coarser grains than the dual phase microstructure shown in cycle 1. This sample achieved the highest elongation compared to the other two cycles. AW-SS heat treated with cycle 3 was austenitized then oil quenched and tempered. The microstructure shows a mixture of ferrite and transformed austenite. The highest ultimate tensile strength and hardness for this alloy was obtained with cycle 3.

The other alloys show a very fine microstructure, which makes it difficult to discern the phases present. The tempered samples have a structure mainly consisting of tempered martensite with varying concentrations of fine carbides in ferrite. The microstructures from cycle 3 are more homogeneous resulting from the high austenitizing temperature used. The melt pool boundaries are no longer visible with this cycle.

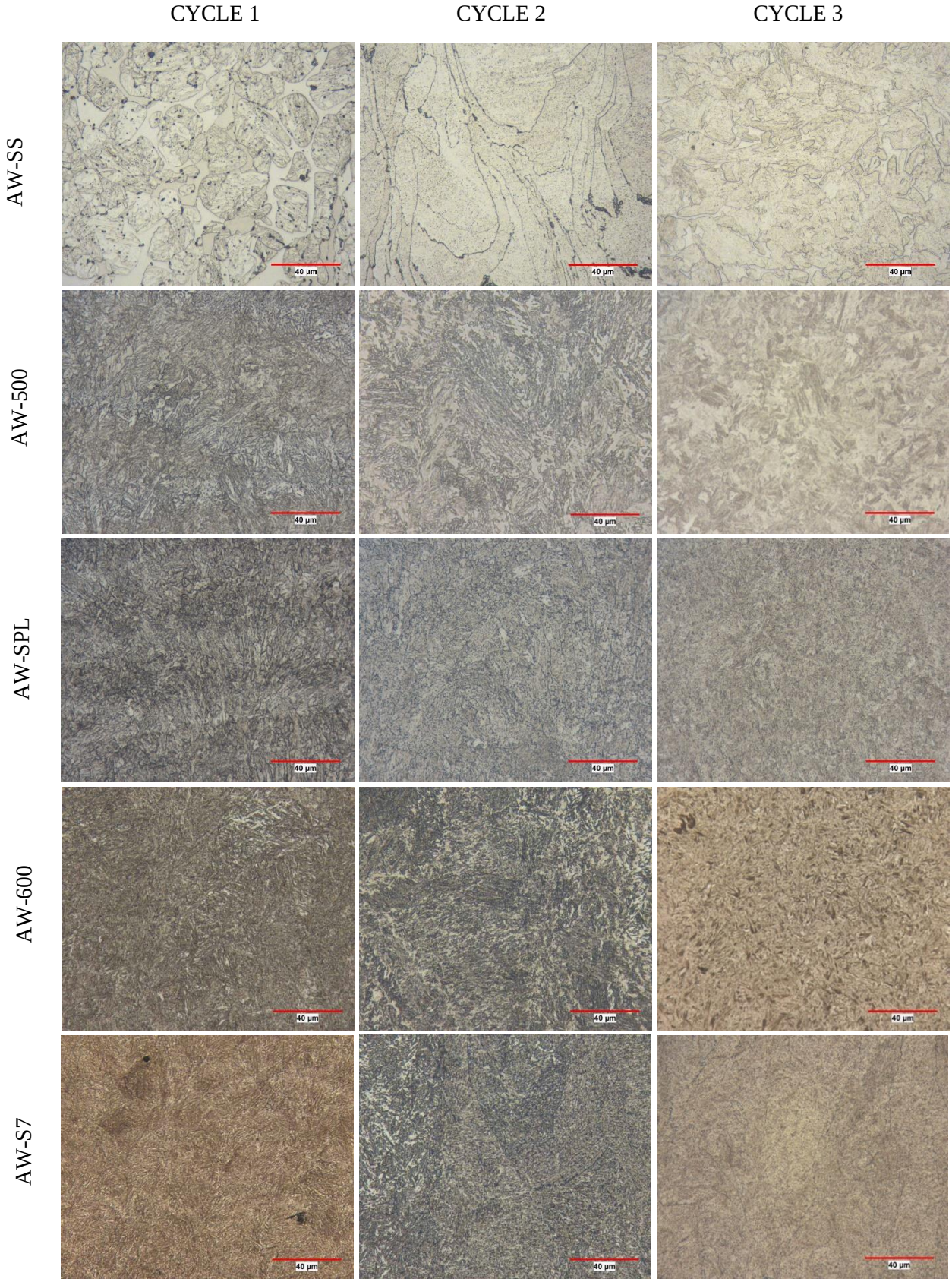

Figure 9. LOM images of AncorWear sample etched microstructures.

Using higher magnifications more detail can be resolved in the fine microstructures of the laser samples and the variation in structure can be seen between the three heat treatments. Figure 10 shows the etched microstructures of AW-500 and AW-600 at higher magnifications.

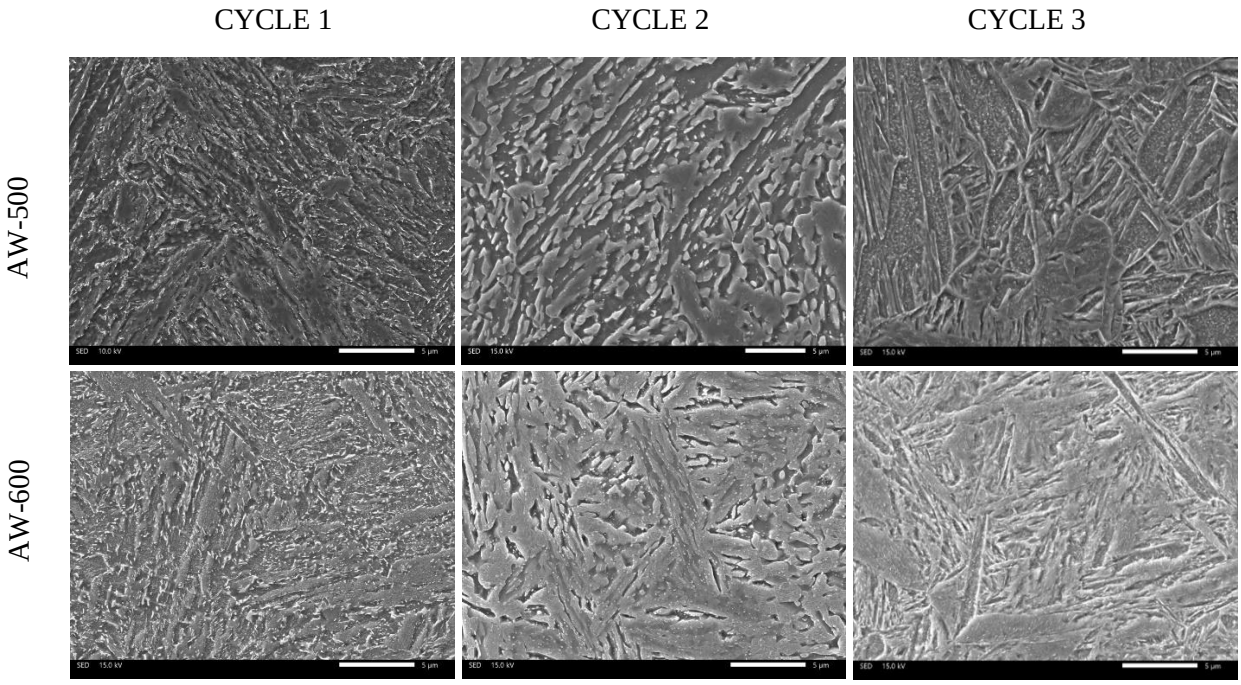

Figure 10. SEM images showing etched microstructures of samples. (*etchant 2 vol % nital, 4 wt% picral)*

Wear Resistance Testing

ASTM G65 abrasion test samples were heat treated according to cycle 1 (593 °C, air cool). Figure 11 shows an image of the sample after testing depicting the wear scar that formed. All alloys showed a similar wear scar. In this test the amount of volume loss correlates to the alloy's wear resistance. Figure 12 shows the volume loss of the alloys ordered from lowest to highest hardness. AW-SS had the highest volume loss while AW-S7 had the lowest. The hardness of the samples did not entirely trend with the volume loss results. Although AW-500 had a lower hardness than AW-600 it had a lower volume loss indicating better wear resistance. Both the AW-500 and AW-SPL samples had a similar volume loss at different hardness levels. The samples were only tested in one heat treatment condition. An optimized heat treatment could further improve each alloy's wear resistance.

Figure 11. Image of abrasion sample after testing.

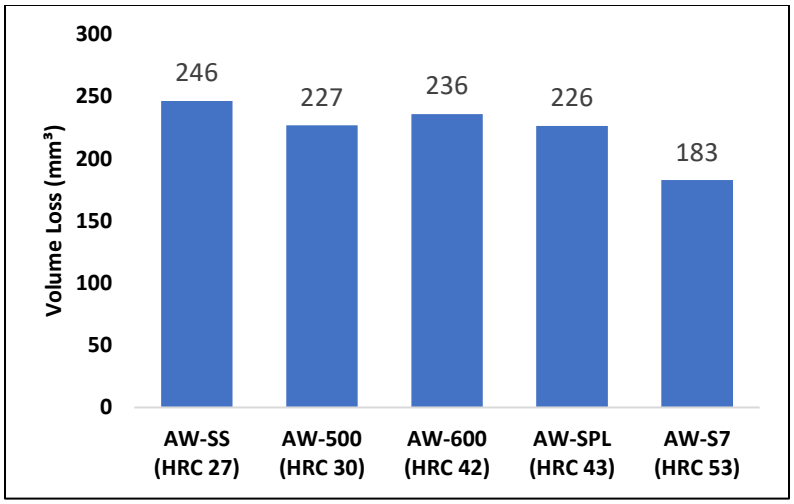

Figure 12. Volume loss results of abrasion test samples.

Figure 13 shows images of samples used for the ASTM G99 pin-on-disk testing. On the left there is an image showing the wear scar formed on the ball and on the right is an image showing the wear scar formed on the disk. The wear scars formed on the balls and disks were different shapes and sizes. Some of the scars appeared to be only surface scratches while others were larger with more material removed indicating a lower resistance to wear.

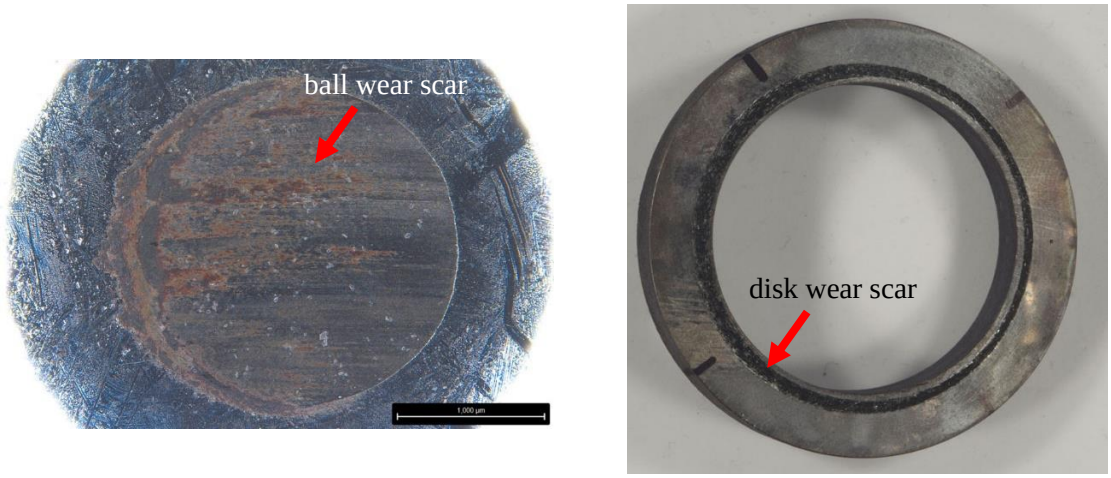

Figure 13. Images of AISI 52100 ball (left) and disk (right) after testing.

Figure 14 shows the average size measurements of the wear scars formed on the ball and disk samples. The size of the wear scar will differ depending on how much wear one component caused on the other. AW-600 and AW-S7 caused the most wear to the ball forming a scar with a 2.18 mm diameter while AW-500 caused the least wear on the ball forming a scar with a 1.08 mm diameter. The diameter of the ball wear scars trends with the hardness of the alloys except for AW-SS. AW-600 had the smallest disk wear scar width at 1.19 mm. The AW-S7 disk wear scar was second largest of the group, which did not follow the trend of increasing hardness. The size measurement of the ball and disk wear scars did not seem to correlate visually to how much wear had occurred. The AW-S7 disk sample appeared to have the least wear of the group. The mass loss from the ball and disk may be a better indicator of wear for these samples. Only one sample was tested of each alloy, so replicate testing may also be needed to confirm the results from this test.

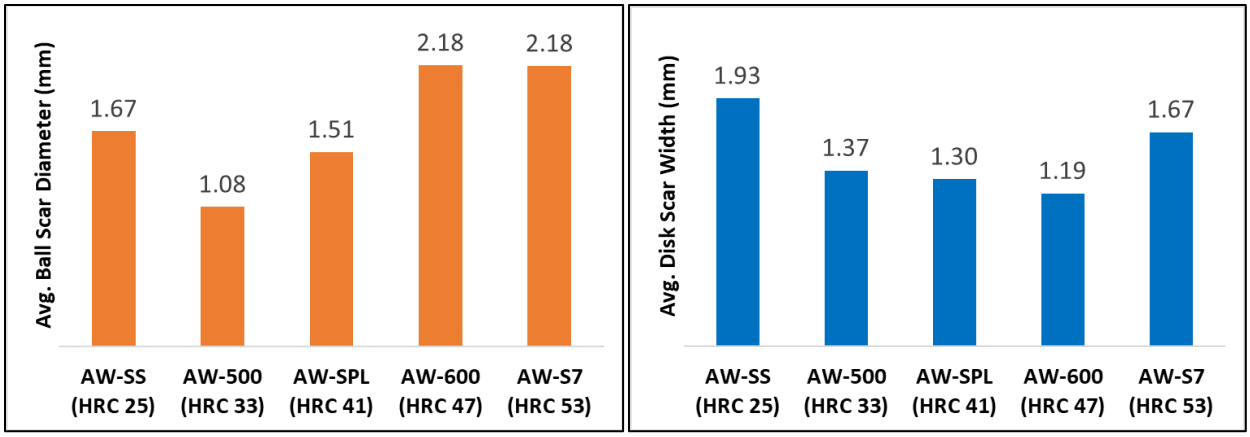

Figure 14. Summary of ball and disk wear scar measurements for AncorWear alloys.

Figure 15 shows SEM images of the surface morphology of the disk wear scars of the AW-600 and AW-SS samples which had the smallest and largest width measurements. At the lower magnification smooth areas can be seen that were untouched by the ball's sliding path. Plastic deformation occurred on the sample surface due to the sliding contact of the ball. The direction of movement of the ball can also be observed. The rougher wear track of the AW-600 is expected due to the sample's higher hardness leading to higher friction between the disk and the ball while the AW-SS shows a less rough wear track due to the material's ductility [2].

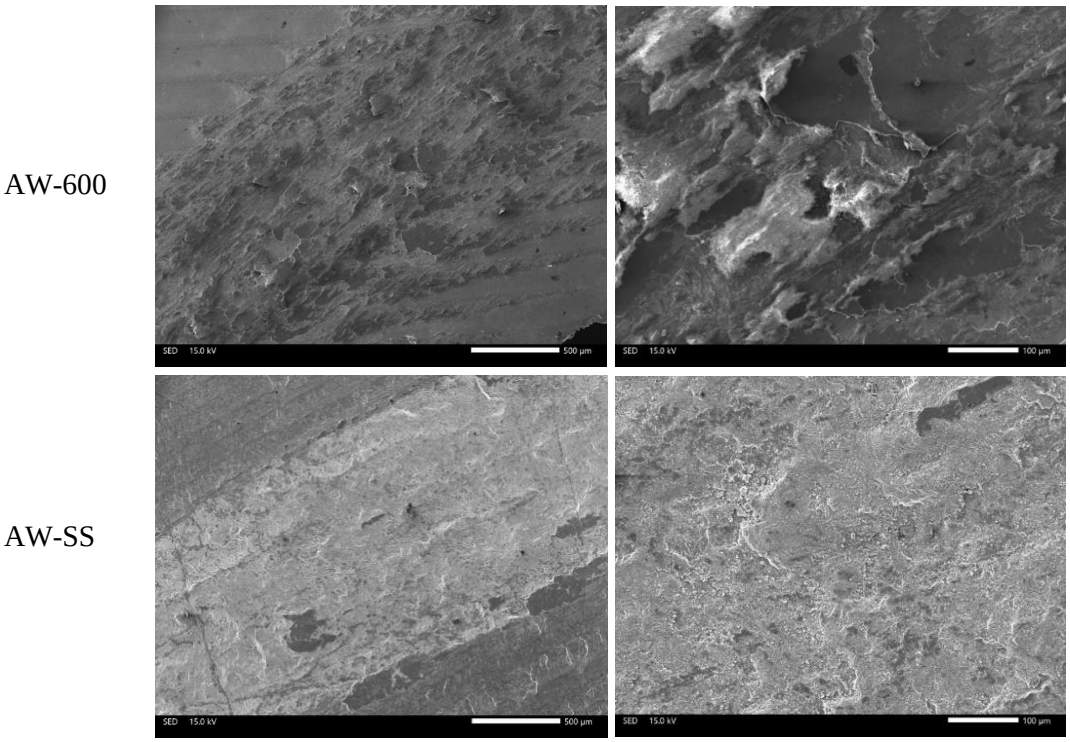

Figure 15. SEM micrographs of AW-600 (top) and AW-SS (bottom) disk wear scars at two magnifications.

CONCLUSIONS

A family of wear-resistant alloys for AM processing have been established. Depending on the application, material selection from these wear-resistant alloys will depend on factors including hardness, toughness, chemical resistance, temperature of operation and environment. AM allows for more design freedom with wear-resistant materials as compared to conventional processing which limits the geometries that can be produced. Mechanical and microstructural properties of printed samples were reviewed. Standardized wear tests were performed to correlate the wear resistance to the hardness and toughness of the materials. The results showed that the hardness of the materials did not entirely trend with the wear testing. Due to the complexity of wear mechanisms standardized testing that most closely matches the application conditions would be recommended when selecting a material. This will help in material development eliminating the need for costly in-process trials. Future work will include wear testing of samples with additional heat treatment conditions as well as varying the testing conditions, such as the specified load and testing temperature.

REFERENCES

1. ASM Handbook Volume 4 Heat Treating, Published by ASM International, 1991.
2. ASM Handbook Volume 18 Friction, Lubrication, and Wear Technology, Published by ASM International, 1992.
3. C. Junghetu, C. Schade, K. Horvay, T. Murphy, "Development of Wear Resistant Alloys for Use in Laser Powder Bed Fusion", *Proceedings of the European Powder Metallurgy Association 2022 Conference.*
4. Standard Test Methods for Metal Powders and Powder Metallurgy Products, 2022, Metal Powder Industries Federation, Princeton, NJ.
5. Standard Test Methods for Notched Bar Impact Testing of Metallic Materials E23-18, published by ASTM International.
6. Standard Test Method for Measuring Abrasion Using the Dry Sand/Rubber Wheel Apparatus G65-16, published by ASTM International.
7. Standard Test Method for Wear Testing with a Pin-on-Disk Apparatus G99-17, published by ASTM International.
8. F. C. Campbell. *Elements of Metallurgy and Engineering Alloys*. 2008, ASM International, Materials Park, Ohio.
9. "S7 Tool Steel–Shock–Resisting Steel (UNS T41907)", AZO Materials, https://www.azom.com/article.aspx?ArticleID=6248
10. T. Murphy, C. Schade, K. Horvay, "Microstructure Development of Dual Phase Stainless Steel Parts Made by Laser Bed Powder Fusion", *Proceedings of the PowdetMet 2021 Conference.*